

# Non-equilibrium Heat Transfer in Acceleration and Pressure-driven Poiseuille Flows: A Comparative Study

Benzi JOHN\*, Xiao-Jun GU, David R. EMERSON

\* Corresponding author: Tel.: ++44 (0)1925 603149; Fax: ++44 (0)1925 603634; Email: benzi.john@stfc.ac.uk

Computational Science and Engineering Department, STFC Daresbury Laboratory, Warrington, UK

**Abstract** A comparison of non-equilibrium flow and heat transfer characteristics between the acceleration-driven and pressure-driven Poiseuille flow is made with the aid of the direct simulation Monte Carlo method. In particular we study thermal characteristics like temperature and heat flux profiles, heat flow rates and net heat flow directions for both cases. Our study shows several interesting similarities and contrarities. Non-equilibrium heat flow phenomenon like a bimodal tangential heat flux profile and a heat flow rate maximum at an intermediate Knudsen number is observed for the case of the pressure-driven flow. For both acceleration and pressure-driven cases, a two-way heat flow is observed in the slip and early transition regime, whereas heat flow is unidirectional in the upper transition regime and beyond. For the pressure-driven Poiseuille flow, the net heat flow is in the opposite direction of mass flow for the entire range of Knudsen number. In the case of the acceleration driven flow, however, the heat flow direction reverses and becomes in the direction of mass flow in the upper transition regime and beyond.

**Keywords:** Non-equilibrium, Poiseuille Flow, Heat flow rate

## 1. Introduction

Study of gaseous flow at micro- and nano-scales is an active area of research today. Several interesting non-equilibrium flow phenomena which are not observable at the continuum level have been revealed from such studies (Gad-el-Hak, 1999; Cercignani, 2000; Karniadakis et al., 2005). It is well known that Navier-Stokes-Fourier based equations have limited capability in predicting non-equilibrium flow and heat transfer phenomenon accurately (e.g. Cercignani and Cortese, 1994; Mansour et al. 1997; Sun and Faghri, 2000; Aoki et al. 2003; Emerson et al. 2007), especially in the transition regime and beyond. The development of computational techniques that can predict the flow accurately under non-equilibrium conditions is important in this context (Reese et al., 2003). Significant efforts have been made recently to extend the hydrodynamic equations to the slip and transition regimes (Grad, 1949; Chapman and Cowling, 1990). The most notable methods include the various well known slip-based

models, the method of moments, and the Burnett equations. Notably, significant progress has been made with regards to the method of moments in modelling non-equilibrium flow in micro geometries. Recent studies (Gu and Emerson 2007, 2010; Torrilhon and Struchtrup 2008) show that the method is able to capture several well known non-equilibrium heat and flow phenomena. High-order models, such as the Burnett equations, can provide improved solutions in the transition region, but they have also been shown to have severe limitations (Bobylev 1982). Another popular method used to model certain prototype micro flows is the linearized Boltzmann equation based methods (Ohwada et al. 1989; Sone et al. 1989), which has been used with a great degree of success even for the case of very high Knudsen number. But they are suitable only for select applications involving extremely low flow-gradients, so that the Boltzmann equation can be linearised around an equilibrium state at rest. This limits its practical use beyond certain ideal flow situations.

Although most of the methods discussed here can provide good approximations, they have only been tested and validated against relatively simple prototype problems or for cases involving comparatively small flow and temperature gradients. Modelling heat transfer calculations under non-equilibrium flow conditions is an added challenge as it depends upon a combination of various factors like compressibility, viscous dissipation, expansion cooling, thermal creep etc. Several anomalous thermal flow features have been reported in literature which the NSF based methods cannot predict even qualitatively. Examples include the bimodal temperature distribution in force-driven Poiseuille flows (Tij and Santos, 1994; Uribe and Garcia, 1999), non-zero tangential heat flux for couette flows (Gu and Emerson, 2009) and counter-gradient heat flux thermal patterns in a lid-driven cavity (John et al. 2010, 2011). Accurate and reliable validation data are invaluable for the development of various computational methods in this context. Experimental methods can provide only limited validation data. Often they can provide only average quantities like mass flow rate, pressure values etc, but they seldom give an accurate representation of detailed velocity or temperature profiles across the channels. The direct simulation Monte Carlo (DSMC) method (Bird, 1994) in this context is not only an accurate and reliable non-equilibrium flow simulation method, but is also a means to provide reliable validation data which helps in the development of alternate computational methods. DSMC is based on the discrete molecular nature of the gas, essentially capturing the physics of a dilute gas governed by the Boltzmann equation.

In the present work we compare the non-equilibrium gaseous flow and heat transfer characteristics of the acceleration-driven and pressure-driven Poiseuille flows. Computations for this have been done using the DSMC method. Plane Poiseuille flows with respect to both the acceleration- and pressure-driven cases are in general well documented in literature. Pressure-driven

Poiseuille flows were studied in Ohwada's work (1989) with the aid of the linearised Boltzmann equation, wherein they studied the heat flow behaviour. However only the tangential heat flux profiles were considered in that work and only three cases of Knudsen number were considered, i.e  $Kn=0.1, 1$  and  $10$ . A more exhaustive study for the case of acceleration-driven flow has been done by Aoki et al. (2002), again using the linearised Boltzmann equation. Uribe and Garcia (1999) studied the acceleration-driven flow using the Burnett equation. Comparisons between DSMC and NSF methods for the case of acceleration- and pressure-driven flows were made by Zheng et al. (2002). However they made comparisons of only velocity, temperature and pressure profiles and considered only the case of  $Kn=0.1$ . In this work we attempt to give a more complete picture of the non-equilibrium heat flow characteristic by studying the thermal characteristics over a wide range of Knudsen number using the DSMC method. Heat flux profiles and detailed thermal flow patterns are investigated for both pressure and force-driven Poiseuille flows.

## 2. DSMC Simulation Method

DSMC is a particle method based on kinetic theory for the simulation of dilute gases. A detailed explanation of the steps involved in the DSMC method can be found in Bird (1994). Starting from a set of initial conditions, the flow develops in a physically realistic manner by evaluating the collisions between the particles and interactions of the particles with solid bodies and inflow/outflow boundaries. Stochastic methods are used to evaluate the collision probabilities and scattering distributions based on kinetic theory. The time step in DSMC simulations being much smaller than the mean collision time, collisions between particles can be decoupled from the positional changes of the particle for each time step.

All the simulations in the present study are performed with a validated parallel DSMC code which has been successfully employed

for various micro-flow simulations (John and Damodaran, 2009a, b; John et al., 2010, 2011). The variable hard sphere (VHS) collision model (Bird, 1994) has been used with a monatomic molecule of mass  $m = 6.63 \times 10^{-26}$  kg, and reference particle diameter of  $d = 4.17 \times 10^{-10}$  m. The particle-wall interactions follow the fully diffuse reflection model. The general guidelines that need to be followed for an accurate DSMC simulation, with respect to the cell size, time step and particle number are well documented in literature (Hadjiconstantinou 2000; Hadjiconstantinou et al., 2003). In the present work, these guidelines have been rigorously followed to ensure the accuracy of the computed flow results. The flow variables are derived as time-averages during the sampling phase, which have been carried out here over a period of several million time steps after the system has reached a steady state.

### 3. Results and Discussion

The configuration of both acceleration and pressure-driven flows is simple. Acceleration-driven flow is essentially one-dimensional. Each particle undergoes an acceleration force in the flow direction. In this work an arbitrary high value of acceleration is specified. To enable a two-dimensional visualization of heat flow in the channel, a two-dimensional DSMC simulation has been done by imposing periodic boundary conditions at the inflow and outflow of the channel. In the case of the pressure-driven flow, the flow is driven by a pressure gradient. The aspect ratio,  $L/H$  considered for the pressure-driven case is 5, wherein  $L$  is the length of the plates and  $H$  is the channel height. Due to symmetry only half the geometry is modeled. A constant pressure ratio of  $P_i/P_o = 1.5$  between the inflow and outflow is maintained for all the cases of  $Kn$ . Here  $P_i$  is the pressure at the inflow of the channel, whereas  $P_o$  is outflow pressure. The wall temperature is set to the reference temperature, i.e.  $T_w = T_0 = 273K$ . Computations have been carried out over various degrees of

non-equilibrium flow conditions quantified by the Knudsen number. The Knudsen number variation is achieved by varying the density conditions in the channel, i.e. the reference pressure,  $P_o$ , at which the simulation is carried out, differs for each  $Kn$ .

#### 3.1 Acceleration-driven Poiseuille Flow

The computed tangential and normal heat flux profiles,  $q_x$  and  $q_y$ , along a vertical line located at a distance of  $2 \times L/3$  from the entrance of the channel is shown in Fig. 1. The heat flux profiles in these plots is non-dimensionalized with respect to the parameter,  $q_0$ , where  $q_0 = \mu R T_0 / L$ .

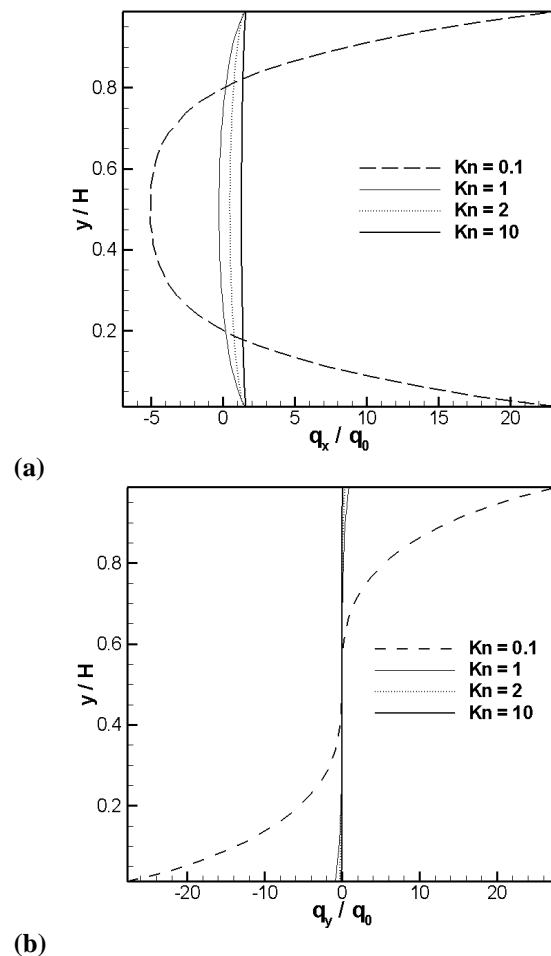


Fig. 1. Variation of computed (a) tangential and (b) normal heat flux profiles,  $q_x$  and  $q_y$  plotted as a function of  $Kn$ .

From the tangential heat profiles, it can be seen at  $Kn=0.1$  and  $Kn=1$ ,  $q_x > 0$  near the walls, while  $q_x < 0$  in the rest of the channel. In the upper transition regime and as the flow approaches the free molecular regime,  $q_x > 0$  in the entirety of the channel, implying that the tangential heat flow direction reverses completely. The normal heat flux profile varies drastically with increase in flow rarefaction. For all cases  $q_y = 0$  along the center of the channel and also in regions close to the channel-center. At  $Kn=0.1$ , the variations in  $q_y$  near the walls are notable and in particular the magnitude of  $q_y$  is significantly higher than that of  $q_x$ . This significantly affects the net heat flow direction near the walls. However for higher values of  $Kn$ , i.e in the upper transition regime and beyond, the variation in  $q_y$  are minimal. This implies that at higher Knudsen numbers, the heat flow in almost the entirety of the channel will be unidirectional. Fig. 2 shows plots of two-dimensional heat flux stream traces overlaid on temperature contours at selected values of  $Kn$  from which thermal patterns and the net gaseous heat transfer direction in the entire channel can be observed.

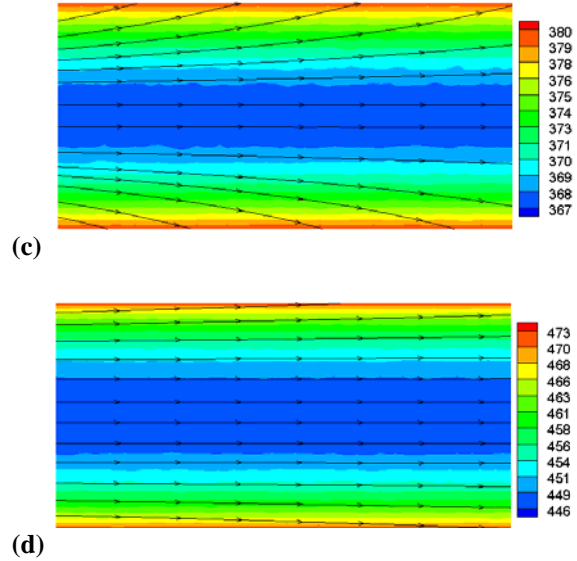
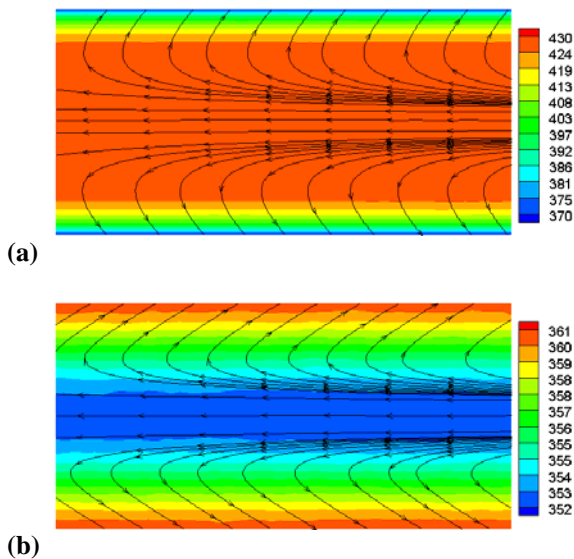
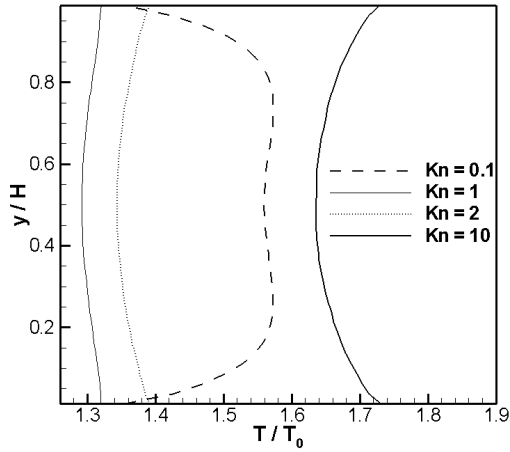
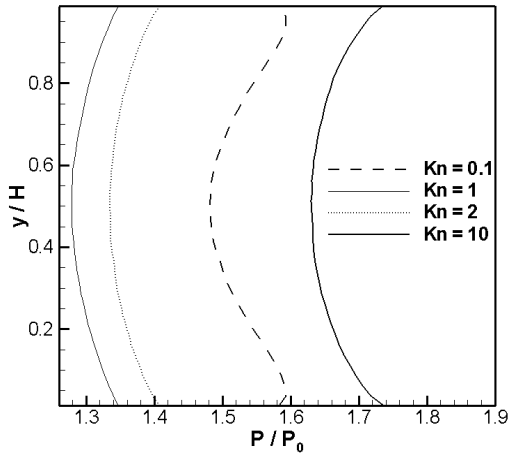


Fig. 2. Comparison of heat flux stream traces overlaid on temperature contours (K) computed for different cases of  $Kn$  (a)  $Kn=0.1$ , (b)  $Kn=1.0$ , (c)  $Kn=2.0$  and (d)  $Kn=10$ .

Two-way heat flow in the slip and early transition regime and the reversal of heat flow at a higher  $Kn$  can be clearly visualized from these plots. The temperature profiles along a vertical line located at a distance of  $2 \times L/3$  from the entrance of the channel are shown in Fig. 3(a). A bimodal trend in temperature is observed at  $Kn=0.1$ , wherein the peak value of gas temperature,  $T$ , is observed away from the walls. At higher values of  $Kn$ , no bimodal trend is observed as the temperature profile characteristics change completely. As the flow approaches the free molecular regime, peak values of gas temperature are observed at the walls. For all the cases of  $Kn$  considered, it is noted the gas temperature along the walls is greater than the wall temperature, i.e.  $T > T_w$ . Near the walls this results in heat transfer from the gas to the wall for all cases. The variation in the pressure profile along a vertical line is shown in Fig. 3(b). It is found that the variation in pressure profile closely follows that of the temperature profile. It is noted that  $P > P_0$  consistently for all values of  $Kn$  considered.



(a)



(b)

Fig. 3. Variation of computed (a) temperature and (b) pressure profiles plotted as a function of Kn.

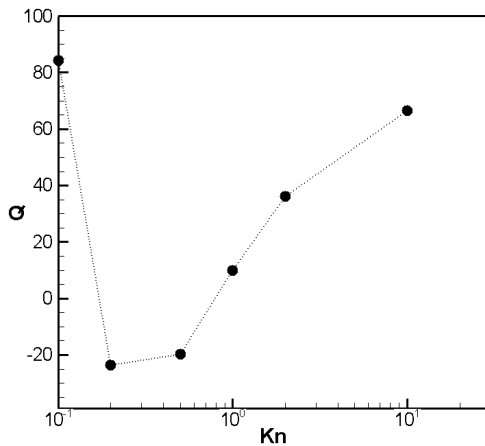


Fig. 4. Predicted heat flow rate plotted as a function of Kn for the acceleration-driven flow.

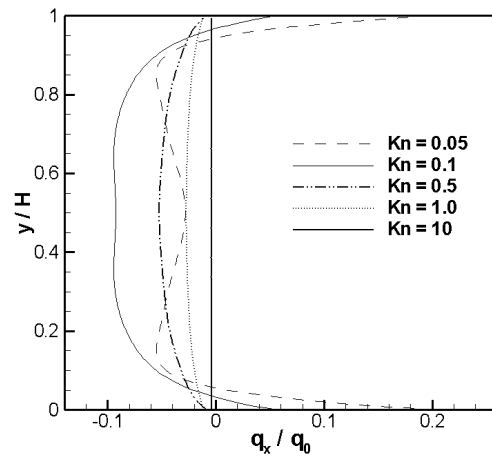
The computed non-dimensional heat flow rate,  $Q$ , as a function of Kn is shown in Fig. 4.

$Q$  is calculated as  $Q = \int_0^H q_x dy / \mu RT_0$ . The

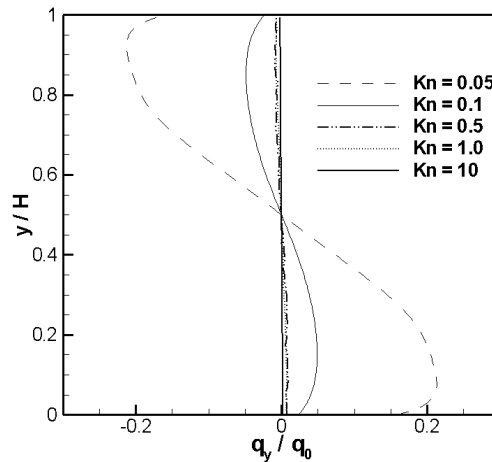
heat flow rate profile shows a dip at an intermediate value of Kn, which in this particular case is at about Kn=0.25. It is interesting to note from the heat flow rate profile that at a particular value of Knudsen number,  $Q=0$  after which it becomes negative. As Kn increases,  $Q > 0$  again and keeps increasing with any further increase in flow rarefaction.

### 3.2 Pressure-driven Poiseuille Flow

The non-dimensional tangential and normal heat flux profiles,  $q_x$  and  $q_y$ , along a vertical line located at a distance of  $2 \times L/3$  from the entrance of the channel for the case of the pressure-driven flow is shown in Fig. 5.



(a)



(b)

Fig. 5. Variation of the (a) tangential and (b) normal heat flux profiles,  $q_x$  and  $q_y$  plotted as a function of Kn.

The heat flux profiles indicate several interesting trends in the heat flow pattern in the channel. As expected the heat flux values decrease with increase in flow rarefaction. This can be attributed due to the fact that collision frequency significantly reduces with increase in flow rarefaction. More interestingly, the tangential heat flux profiles reveal a bimodal shape with a dip in the center in the slip and early transition regimes. The bimodal shape, however, diminishes with increasing Kn as the profiles follow a parabolic pattern in the upper transition regime and beyond. The computed heat flux profiles show that similar to the acceleration-driven case,  $q_x > 0$  near the walls, from the slip to the early transition regime. However away from the walls,  $q_x$  takes negative values consistently for all cases of Kn.

The predicted normal heat flux,  $q_y$  profiles are shown in Fig. 5(b). The trends are quite similar to those observed for the acceleration-driven case. However the reduction in  $q_y$  profiles observed for the case of the pressure-driven flow is not as drastic as that for the acceleration-driven case. For all cases of Kn considered,  $q_y = 0$  along the center of the channel. Again this indicates that along the center of the channel the heat flow will be unidirectional, where as near the walls the heat flow gets affected by the gas-wall interactions. This is particularly true at relatively low Knudsen numbers, wherein the magnitude of  $q_y$  is much higher compared to that of  $q_x$ . Net heat flow in this case will be in the y-direction. Heat flow along the center of the channel will always be in the x-direction regardless of Kn. In the upper transition regime and in the free molecular regime, heat flow will be consistently unidirectional which is in the opposite direction of mass flow in almost the entirety of the channel. These thermal patterns and the net gaseous heat transfer direction in the entire channel can be clearly visualized from Fig. 6, which shows plots of two-dimensional heat flux stream traces overlaid on temperature contours at

selected values of Kn. From the temperature contours it is observed that there is a drastic drop in temperature towards the channel outlet. This can be attributed due to the sudden flow expansion and pressure drop at outlet. Peak values of temperature are located near the walls, whereas minimum values of temperature are observed along the channel-center. As expected, the temperature variations along the channel are minimal in the upper transition regime and the free molecular regime, compared to those at lower Kn. It is noted that along the walls, the gas temperature is less than the wall temperature, i.e.  $T < T_w$  for all the cases of Kn considered. Apparently this is caused by a drop in pressure along the length of the channel. This leads to an expansion cooling phenomenon near the walls which results in heat transfer from the wall to gas, unlike for the case of the force-driven case, where close to the wall the heat flow is from the gas to the wall.

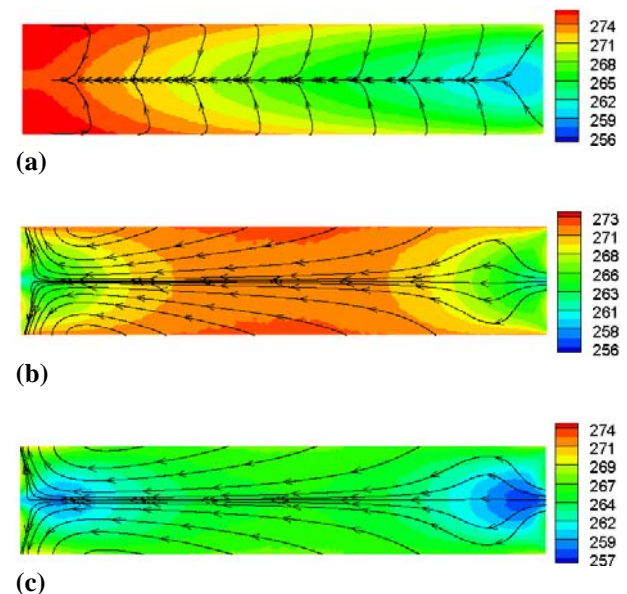


Fig. 6. Comparison of heat flux stream traces overlaid on temperature contours (K) computed at  $P_i/P_o = 1.5$  for different cases of Kn (a) Kn=0.05, (b) Kn=1.0 and (c) Kn=10.

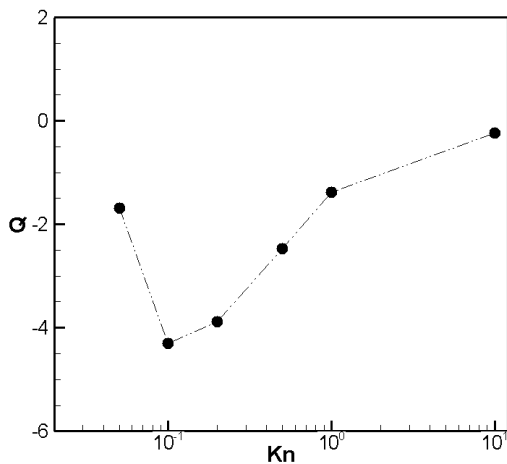


Fig. 7. Predicted heat flow rate plotted as a function of Kn for the pressure-driven flow.

The non-dimensional heat flow rate,  $Q$  computed as a function of Kn for the pressure-driven Poiseuille flow is shown in Fig. 7. It is interesting to note that similar to the acceleration-driven case, the heat flow rate profile exhibits a dip at an intermediate value of Kn (in this particular case at about  $Kn=0.1$ ). However, in contrast,  $Q < 0$  consistently for all cases of Kn for the pressure-driven case, mainly due to the fact that heat flow is largely in the opposite direction of mass flow. Hence it is noteworthy that when considered in terms of magnitude, it is actually a heat flow maximum that is observed in the case of the pressure-driven flow.

#### 4. Conclusions

A comparative study for the non-equilibrium heat transfer between the acceleration-driven and pressure-driven Poiseuille flow has been made in this work. Thermal characteristics have been studied over a wide range of Knudsen number with the aid of the direct simulation Monte Carlo method. The computed results indicate several interesting similarities and contrarities between the two cases. It is found that thermal characteristics for the acceleration-driven case changes drastically with increase in flow rarefaction. Temperature profile both in terms of magnitude and trends vary notably. In contrast, for the pressure-driven case, temperature variations with increase in flow rarefaction are not that drastic. For both cases, the tangential

heat flux is positive near the walls in the slip and early transition regime. The normal heat flux profile near the walls is significant compared to the tangential heat flux profile, significantly affecting the net heat flow direction near the walls for both cases. For the pressure-driven case, the net heat flow for all cases, in general, is largely in a direction opposite to that of the mass flow for all values of Knudsen number. For the acceleration-driven case, the net heat transfer direction reverses totally as the flow approaches the upper transition and free molecular regime and becomes consistently in the direction of mass flow. A pressure drop in the flow direction for the pressure-driven Poiseuille flow results in an expansion cooling phenomenon near the walls, leading to heat transfer from the walls to the gas. In the acceleration-driven case, however, the heat transfer near the walls is from the gas to the wall. Also interestingly, the non-dimensional heat flow rate profiles for both acceleration- and pressure-driven flow show a unique value at an intermediate value of Kn, at which the heat flow rate exhibits a minimum or a maximum value. Lastly, the present work provides ample scope for further study. The effect of acceleration for the forced-driven flow and pressure ratio for the pressure-driven flow, on the non-equilibrium heat transfer characteristics is interesting and is being carried out currently.

#### Acknowledgements

The authors would like to thank the Engineering and Physical Sciences Research Council (EPSRC) for their support of Collaborative Computational Project 12 (CCP12).

#### References

- Aoki, K., Takata, S., Nakanishi, T., 2002. Poiseuille-type flow of a rarefied gas between two parallel plates driven by a uniform external force. *Phys. Rev. E* 65, 026315.
- Aoki, K., Yoshida, H., Nakanishi, T., Garcia, A.L., 2003. Inverted velocity profile in the cylindrical couette flow of a rarefied gas. *Phys. Rev. E* 68, 016302.
- Bird, G., 1994. *Molecular Gas Dynamics and the Direct Simulation of Gas Flows*. Clarendon Press, Oxford.
- Bobylev, A. V., 1982. *The Chapman-Enskog and*

- Grad methods for solving the Boltzmann equation. *Sov. Phys. Dokl.* 27, 29-31.
- Cercignani, C., Cortese, S., 1994. Validation of a Monte Carlo simulation of the plane Couette flow of a rarefied gas. *J. Stat. Phys.* 75, 817-838.
- Cercignani, C., 2000. *Rarefied Gas Dynamics: From Basic Concepts to Actual Calculations.* Cambridge University Press, Cambridge.
- Chapman, S., Cowling, T.G., 1990. *The Mathematical Theory of Non-Uniform Gases.* Cambridge University Press, Cambridge.
- Emerson, D.R., Gu, X.J., Stefanov, S.K., Yuhong, S., Barber, R.W., 2007. Nonplanar oscillatory shear flow: From the continuum to the free-molecular flow. *Phys. Fluids* 19, 107105.
- Gad-el-Hak, M., 1999. The fluid mechanics of microdevices - The Freeman scholar lecture. *J. Fluids Eng.* 121, 5-33.
- Grad, H., 1949. On the kinetic theory of rarefied gases. *Commun. Pure Appl. Math.* 2, 331-407.
- Gu, X.J., Emerson, D.R., 2007. A computational strategy for the regularized 13 moment equations with enhanced wall-boundary conditions. *J. Comput. Phys.* 225, 263-283.
- Gu, X.J., Emerson, D.R., 2009. A high-order moment approach for capturing non-equilibrium phenomena in the transition regime. *J. Fluid Mech.* 636, 177-216.
- Hadjiconstantinou, N. G., 2000. Analysis of discretization in the direct simulation Monte Carlo. *Phys. Fluids* 12, 2634-2638.
- Hadjiconstantinou, N. G., Garcia, A. L., Bazant, M. Z., He, G., 2003. Statistical error in particle simulations of hydrodynamic phenomena. *J. Comput. Phys.* 187, 274-297.
- John, B., Damodaran, M., 2009. Computation of head-disk interface gap micro flowfields using DSMC and continuum-atomistic hybrid methods. *Int. J. Numer. Meth. Fluids* 61, 1273-1298.
- John, B., Damodaran, M., 2009. Hybrid continuum-direct simulation Monte Carlo and particle-laden flow modelling in the head-disk interface gap. *IEEE Trans. Magn.* 45, 4929-4932.
- John, B., Gu, X.J., Emerson, D.R., 2010. Investigation of heat and mass transfer in a lid-driven cavity under non-equilibrium flow conditions. *Numer. Heat Transf. B* 58, 287-303.
- John, B., Gu, X.J., Emerson, D.R., 2011. Effects of incomplete surface accommodation on non-equilibrium heat transfer in cavity flow: A parallel DSMC study. *Comput. Fluids* 45, 197-201.
- Karniadakis, G., Beskok, A., Aluru, N., 2005. *Microflows and Nanoflows: Fundamentals and Simulation.* Springer, New York.
- Mansour, M.M., Baras, F., Garcia, A., 1997. On the validity of hydrodynamics in plane Poiseuille flows. *Physica A* 240, 255-267.
- Ohwada, T., Sone, Y., Aoki, K., 1989. Numerical analysis of the Poiseuille and thermal transpiration flows between two parallel plates on the basis of the Boltzmann equation for hard-sphere molecules. *Phys. Fluids A* 1(12), 2042-2049.
- Reese, J.M., Gallis, M.A., Lockerby, D.A., 2003. New directions in fluid dynamics: non-equilibrium aerodynamic and microsystem flows. *Phil. Trans. R Soc. Lond. A* 361, 2967-2988.
- Sone, Y., Ohwada, T., Aoki, K., 1989. Temperature jump and Knudsen layer in a rarefied gas over a plane wall: Numerical analysis of the linearized Boltzmann equation for hard sphere molecules. *Phys. Fluids A* 2, 363-370.
- Struchtrup, H., Torrilhon, M., 2003. Regularization of Grad's 13 moment equations: derivation and linear analysis. *Phys. Fluids* 15, 2668-2680.
- Sun, H., Faghri, M., 2000. Effects of rarefaction and compressibility of gaseous flow in microchannel using DSMC. *Numer. Heat Transf. A* 38, 153-168.
- Tij, M., Santos, A., 1994. Perturbation analysis of a stationary nonequilibrium flow generated by an external force. *J. Stat. Phys.* 76, 1399-1414.
- Torrilhon, M., Struchtrup, H., 2008. Boundary conditions for regularized 13-moment-equations for micro-channel-flows. *J. Comput. Phys.* 227, 1982-2011.
- Uribe, F., Garcia, A., 1999. Burnett description for plane Poiseuille flow. *Phys. Rev. E* 60, 4063-4078.
- Zheng, Y., Garcia, A., Alder, B., 2002. Comparison of kinetic theory and hydrodynamics for Poiseuille flow. *J. Stat. Phys.* 109, 495-505.